Supporting Information

In-situ regulation of dendrite-free lithium anode by improved solid electrolyte interface with defect-rich boron nitride quantum dots

Jun Pu,[a,d] Pan Xue,[b] Taotao Li,[b] Jianghua Wu,[b] Kai Zhang,[b] Kaiping Zhu,[b] Shaohua Guo,[b] Guo Hong,[a,] Haoshen Zhou,[c,]* and Yagang Yao,[b,]**

[a] Department of Materials Science and Engineering, College of Engineering, City University of Hong Kong, 83 Tat Chee Avenue, Kowloon, Hong Kong SAR 999077, China

[b] National Laboratory of Solid State Microstructures, College of Engineering and Applied Sciences, Jiangsu Key Laboratory of Artificial Functional Materials, Collaborative Innovation Center of Advanced Microstructures, Nanjing University, Nanjing 210093, China

[c] Graduate School of System and Information Engineering, University of Tsukuba, 1-1-1, Tennoudai, Tsukuba 305-8573, Japan

[d] Key Laboratory of Functional Molecular Solids, Ministry of Education, College of Chemistry and Materials Science, Anhui Normal University, Wuhu 241002, P.R. China

* Corresponding author

Guo Hong: E-mail: galen.hong@gmail.com

Haoshen Zhou: E-mail: hs.zhou@aist.go.jp

Yagang Yao: E-mail: ygyao2018@nju.edu.cn

Experimental Section

Density functional theory calculation:

The Li-ion adsorption on different BN materials was modeled using the CASTEP code.[1] In geometric optimization and energy calculation, the cutoff energy of the plane-wave bases was set to 500 eV. The Perdew-Burke-Ernzerh of version of the generalized gradient approximation was used to describe exchange correlation effects.[2,3] The Brillouin zone was sampled using a 3×3×1 Monkhorst-Pack mesh k-points. The binding energy (E_b) was defined as:

$$E_b = E_{sub} + E_{Li} - E_{sub+Li}$$

where the E_{sub+Li}, E_{sub}, and E_{Li} represent the ground-state energies of the substrate-Li, substrate, and Li-ion, respectively. The diffusion barrier of Li on the surfaces of different substances was evaluated by transitional state locating using the Nudged-Elastic-Band method.[4,5]

COMSOL simulation:

The simulations were carried out on COMSOL Multiphysics 6.0 with implemented finite element solver. The electrolytic liquid was subject to the standard 1 M LiTFSI system, and the Li-ion diffusion coefficient and electrolyte conductivity were 1.5×10^{-10} m S^{-2} and 10^{-2} S cm^{-1}, respectively.[6] The current density of metallic Li electrochemical deposition was 10 mA cm^{-2}. Initial surface protuberances were introduced in the bare Li mode as Li dendrites to simplify the computation process.[7]

Figures:

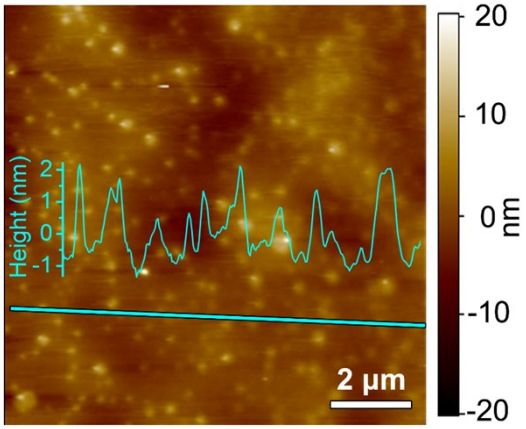

Fig. S1. AFM image of the BN nanosheets precursor and corresponding thickness profile along the line.

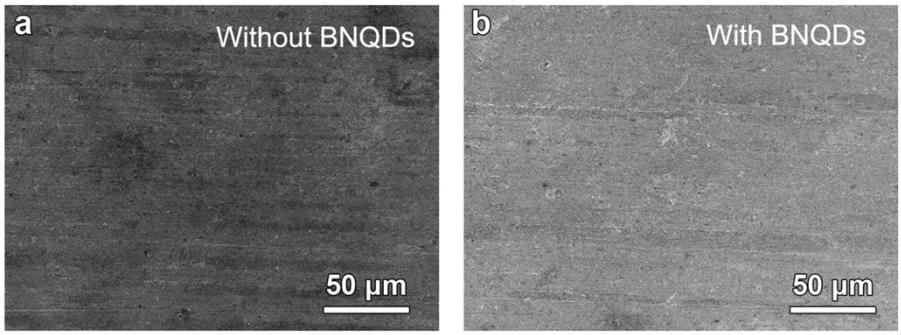

Fig. S2. SEM images of bare Cu foil and the as-prepared Cu with BNQDs electrodes, respectively.

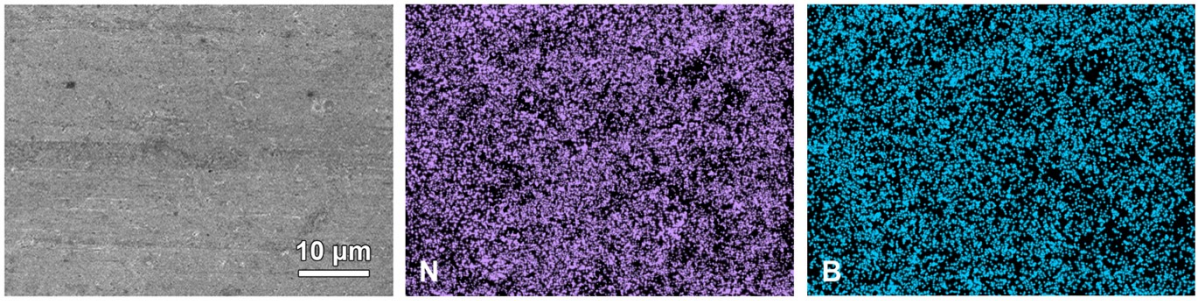

Fig. S3. Elemental mappings of the as-obtained electrode with BNQDs.

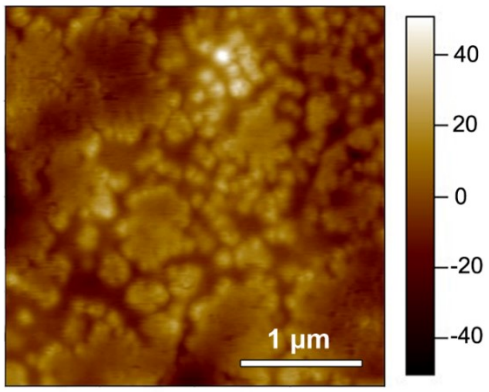

Fig. S4. AFM image of the BNQDs layer on Cu foil (the edge).

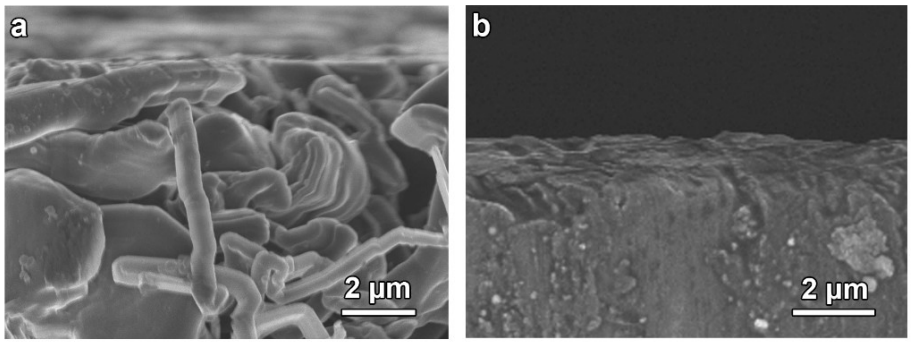

Fig. S5. Localized high-magnification SEM images of Li deposition in cross section: (a) without BNQDs, (b) with BNQDs.

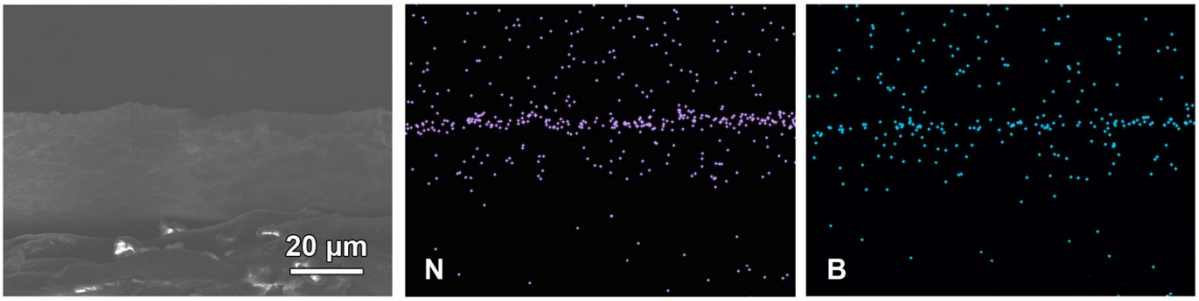

Fig. S6. Cross-section SEM image of cycled Li deposits with BNQDs and corresponding element mappings of B and N.

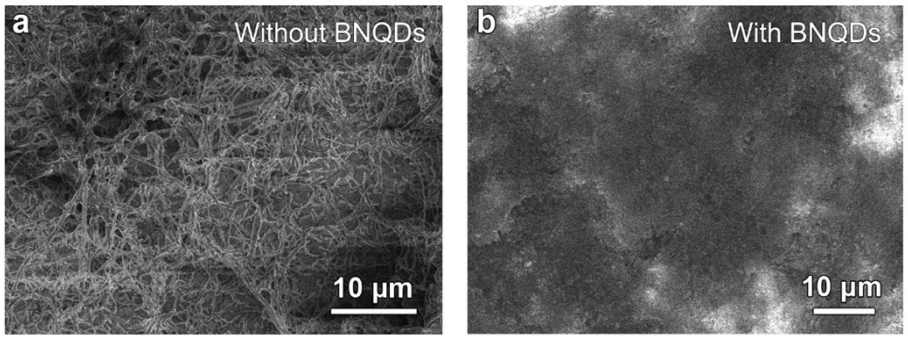

Fig. S7. Top suface SEM images of current collectors after Li stripping: (a) without BNQDs, (b) with BNQDs.

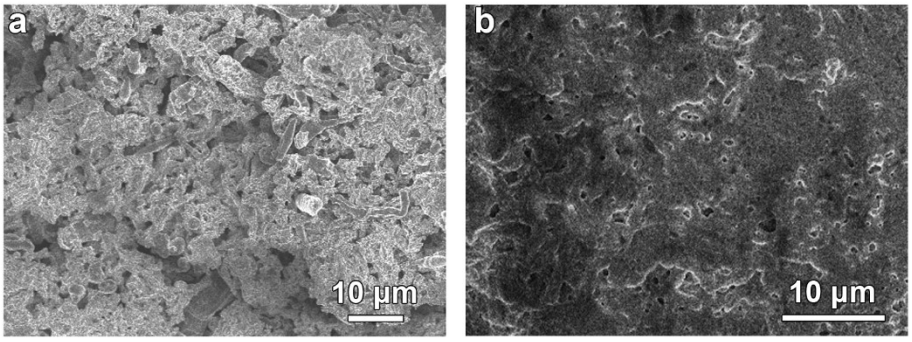

Fig. S8. Top surface SEM images of Li deposition after 50 cycles: (a) without BNQDs, (b) with BNQDs.

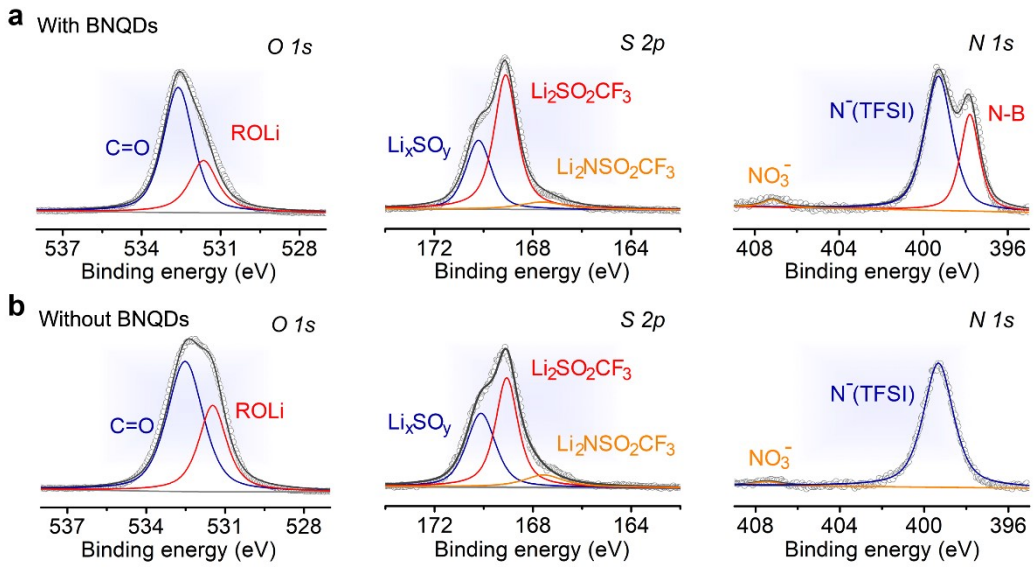

Fig. S9. The O 1s, S 2p, and N 1s high-resolution XPS comparison of the SEI on Li surface with (a) and without (b) BNQDs after cycling.

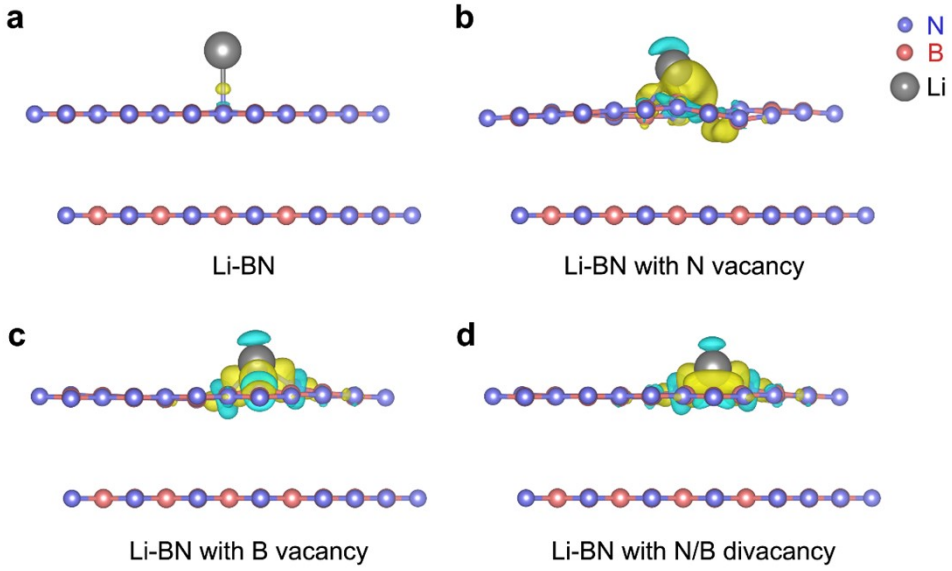

Fig. S10. The side view optimized adsorption configuration and charge differential density images for Li on different BN substrates: (a) initial BN, (b) BN with N vacancy, (c) BN with B vacancy, and (d) BN with N, B vacancy.

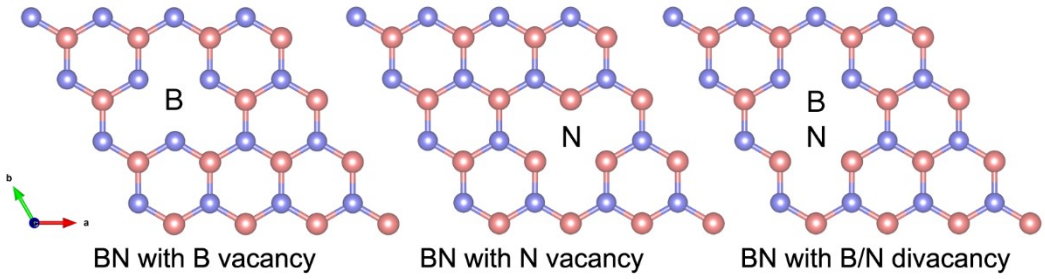

Fig. S11. Schematic diagrams of BN nanostructure with different defects.

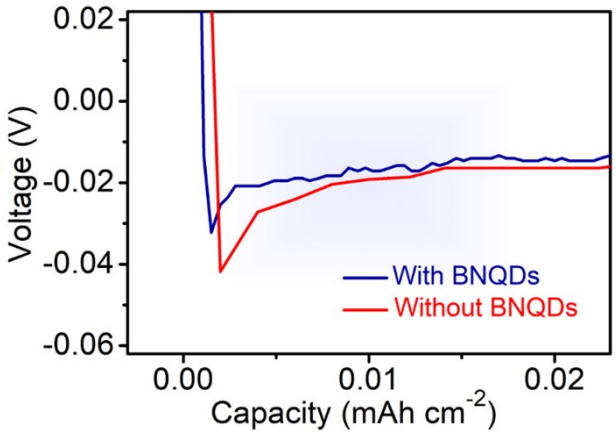

Fig. S12. Voltage profiles of Li electrodepositing on the Cu foils with and without BNQDs at 0.5 mA cm^{-2}.

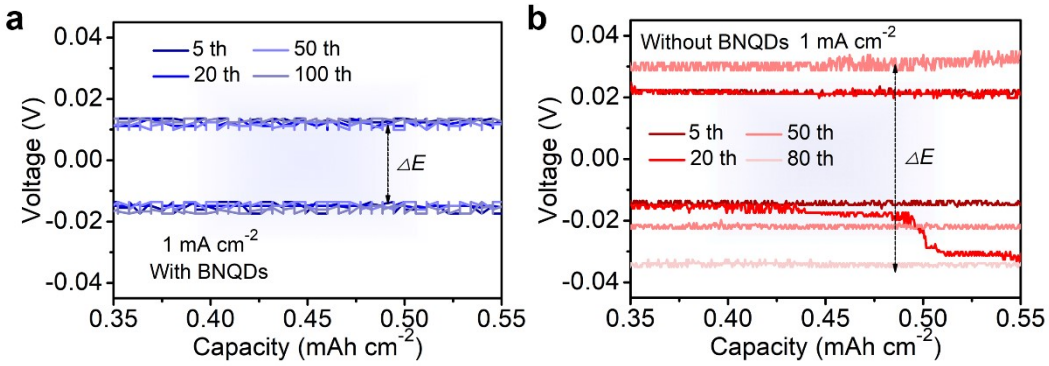

Fig. S13. Locally amplified voltage distribution of Li/Cu half cells at different cycles: (a) with BNQDs, (b) without BNQDs.

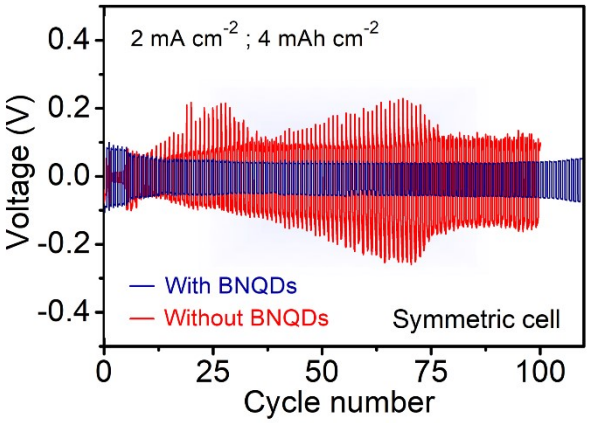

Fig. S14. Cycling stability of symmetric cells with a higher rate of 2 mA cm^{-2} and a limited capacity of 4 mAh cm^{-2}.

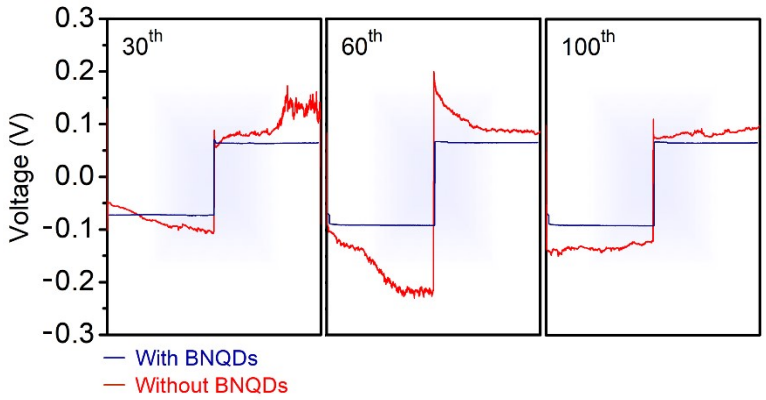

Fig. S15. Detailed voltage profiles of the symmetric cells at 30th, 60th, and 100th cycles.

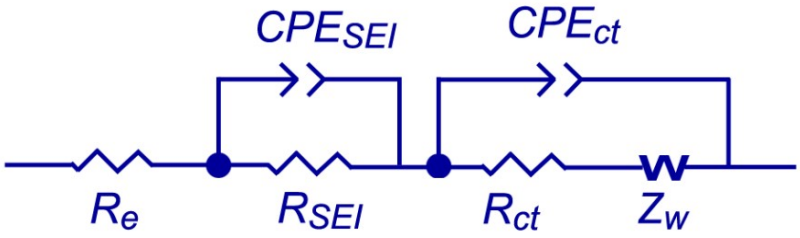

Fig. S16. Equivalent circuit for impedance fitting.

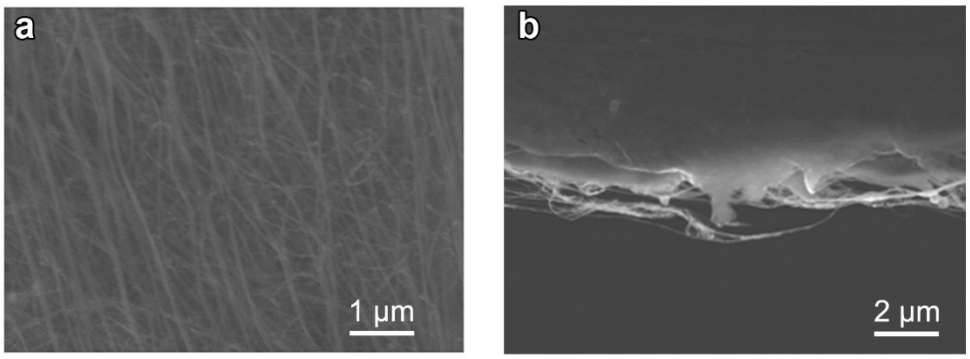

Fig. S17. The SEM images of CNT physical barrier as lithium polysulfides in Li–S full cells.

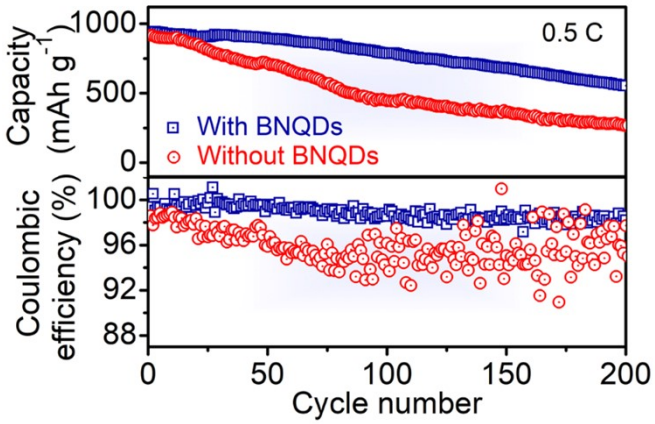

Fig. S18. Cycling performance of Li–S full batteries with and without BNQDs at 0.5 C.

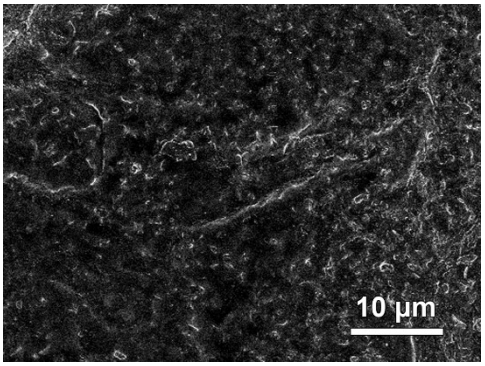

Fig. S19. SEM image of cycled Li anode with BNQDs in Li–S full cell.

References

[1] S. J. Clark, M. D. Segall, C. J. Pickard, P. J. Hasnip, M. I. J. Probert, K. Refson, M. C. Payne, *Z. Kristallogr. - Cryst. Mater.*, 2005, **220**, 567−570.

[2] J. P. Perdew, K. Burke, M. Ernzerhof, *Phys. Rev. Lett.*, 1996, **77**, 3865−3868.

[3] S. Grimme, *J. Comput. Chem.*, 2006, **27**, 1787−1799.

[4] G. Henkelman, H. Jónsson, *J. Chem. Phys.*, 2000, **113**, 9978−9985.

[5] G. Henkelman, B. P. Uberuaga, H. Jónsson, *J. Chem. Phys.*, 2000, **113**, 9901−9904.

[6] J. Y. Wu, X. W. Li, Z. X. Rao, X. N. Xu, Z. X. Cheng, Y. Q. Liao, L. X. Yuan, X. L. Xie, Z. Li, Y. H. Huang, *Nano Energy*, 2020, **72**, 104725.

[7] L. Ye, M. Liao, X. R. Cheng, X. F. Zhou, Y. Zhao, Y. B.Yang, C. Q. Tang, H. Sun, Y. Gao, B. J. Wang, H. S. Peng, *Angew. Chem. Int. Ed.*, 2021, **60**, 17419–17425.